Materials Advances

ROYAL SOCIETY OF CHEMISTRY

PAPER

View Article Online
View Journal | View Issue

Check for updates

Cite this: *Mater. Adv.*, 2024, 5, 3696

One action, two benefits: improving the performance of lithium–sulfur batteries with a poly(ionic liquid)†

Sixin Jia,‡[a] Rui Wang,‡[a] Fengquan Liu,*[b] Hong Huo,[a] Jianjun Zhou*[a] and Lin Li*[ab]

Lithium–sulfur (Li–S) batteries have been considered as one of the most promising candidates for high energy-density batteries due to their high theoretical capacity (1675 mA h g^{-1}). However, the cycling performance is not satisfactory due to the "shuttle effect" of polysulfide and the growth of Li dendrites. In this study, imidazole-based poly(ionic liquid) (PIL) is synthesized. Using PIL in Li–S batteries, we realize the goal of achieving two benefits with one action. The cross-linked PIL (c-PIL) is used to modify the S cathode, and the shuttling of polysulfides is effectively inhibited due to the strong adsorption capability. Density functional theory (DFT) calculations indicate that the strong van der Waals and electrostatic interaction promote the adsorption of polysulfides. PIL, as an artificial solid electrolyte interface layer, is coated on the Li anode to prevent the corrosion of liquid electrolyte and homogenize Li^+ flux. The results of DFT and X-ray photoelectron spectroscopy indicate that the N containing imidazole in PIL can be reduced by active Li to form a Li_3N rich layer on the interface. The Li_3N containing interfacial layer can promote dendrite-free Li deposition beneath the PIL coating layer. By functionalizing the S cathode and Li anode, the PIL@Li‖c-PIL@S batteries show much improved cycling stability and C-rate performance. The results manifest that our strategy of modification of the cathode and anode electrodes is effective, which is sure to promote the development of advanced Li–S batteries.

Received 5th February 2024,
Accepted 2nd March 2024

DOI: 10.1039/d4ma00115j

rsc.li/materials-advances

Open Access Article. Published on 07 March 2024. Downloaded on 2/7/2026 9:32:35 PM.
This article is licensed under a Creative Commons Attribution-NonCommercial 3.0 Unported Licence.

1 Introduction

Lithium–sulfur (Li–S) batteries have been considered as one of the most promising candidates for high energy-density batteries due to high energy density (2600 W h kg^{-1}) and theoretical capacity (1675 mA h g^{-1}) as well as abundant sulfur resources.[1,2] However, the widespread application of Li–S battery still suffers from some defects, such as the "shuttle effect" of soluble lithium polysulfide (LiPS) and the growth of Li dendrites during cycling.[3,4] The shuttling of LiPS results in the loss of active substances in the cathode, and its reduction leads to the formation of an insulation layer on the surface of Li metal anode,[5,6] which deteriorate the cycling stability due to the continuously increased interfacial polarization.[7,8] Meanwhile, Li dendrites have high reaction activity. It reacts with liquid electrolyte (LE), which consumes LE continuously, unable to form stable solid electrolyte interface (SEI) layer on the Li anode.[9,10] LE depletion accompanied by the pulverization of the Li anode will result in fast capacity diving of Li–S batteries. Therefore, great efforts have been made to inhibit the shuttling of LiPS and protect the Li metal anode by promoting the formation of a stable SEI layer.

Numerous efforts have been made to inhibit the shuttling of LiPS.[11,12] Among them, ionic liquids (ILs), composed entirely of cations and anions, are very unique, since they have high ionic conductivity and large adsorption capacity due to their high charge density and strong electrostatic interaction.[13–15] It is generally accepted that the incorporation of IL moieties into the polymer chain combines some of the unique characters of ILs with the common features of polymers. With ILs as side groups, poly(ionic liquid)s (PILs) inherit most of the advantages of ILs, especially the large adsorption capacity.[16–18] Therefore, PILs are supposed to be good candidates for the absorption of polysulfides.[19,20] Studies have shown that some strategies using PIL can effectively enhance the adsorption of polysulfide species in the electrolytes to improve the electrochemical performance of Li–S batteries, such as rational regulation of polysulfide behaviors with a polymeric zwitterion,[21]

[a] *Beijing Key Laboratory of Energy Conversion and Storage Materials, College of Chemistry, Beijing Normal University, Beijing 100875, P. R. China. E-mail: lilinll@bnu.edu.cn, pla_zjj@bnu.edu.cn*
[b] *College of Textile & Clothing, State Key Laboratory of Bio-Fibers and Eco-Textiles, Qingdao University, Qingdao, 266071, P. R. China. E-mail: fqliu@qdu.edu.cn*

† Electronic supplementary information (ESI) available. See DOI: https://doi.org/10.1039/d4ma00115j

‡ These authors contributed equally to this work.

© 2024 The Author(s). Published by the Royal Society of Chemistry

Open Access Article. Published on 07 March 2024. Downloaded on 2/7/2026 9:32:35 PM. This article is licensed under a Creative Commons Attribution-NonCommercial 3.0 Unported Licence.

functionalizing the PE separator with PIL[22] or using PIL containing sandwich-type functional nanomats.[23] The PIL layers can effectively inhibit the diffusion of polysulfides to the anode and hinder their shuttling. However, the dissolution of polysulfides into the electrolyte and loss of active material are still very significant. Incorporating PIL into the cathode seems effective in suppressing the shuttle effect of polysulfides, since the cation on PIL can absorb them once dissolved into the liquid electrolyte.[24] Using multi-arm PILs or cross-linked PILs can further enhance the adsorption capability on polysulfides.[25,26] Therefore, the subsequent research will primarily focus on modifying the S cathode with cross-linked PILs to improve the cycling performance of Li–S batteries.

A stable SEI film on the Li metal anode is a prerequisite for Li–S batteries to achieve stable long-term cycling performance.[27] The SEI film can be optimized by adding additives in liquid electrolyte,[28,29] using a functionalized separator[30,31] or directly coating an artificial SEI film on Li foil.[32,33] The SEI film is an electronic insulated but ionic conductive layer.[34] Most polymers are electronically insulated, and a variety of polymers have been used to form artificial SEI films on the Li foil surface.[35,36] Due to the fact that most of the polymers are not good ionic conductor, PILs have attracted great interest as part of artificial SEI films. Wu *et al.*[37] reported the utilization of a cationic PIL-based solid polymer electrolyte, which exhibited enhanced dissociation of Li^+ ions compared to neutral polymers due to Coulombic interaction with anions of lithium salt, thereby facilitating efficient Li^+ transportation. Liao *et al.*[38] synthesized a new type of bi-functional PIL by a double-crosslinking method, in which partial cations are involved in the formation of the SEI layer on Li metal, thereby effectively preventing the reaction between the electrolyte and the electrode and suppressing the growth of Li dendrites. Huang *et al.*[39] reported a PIL layer to enable air-stable, dendrite-free, and high capacity Li metal anodes by coating poly(diallyl dimethyl ammonium)-TFSI directly on Li metal. The polymeric cations provide an electrostatic shielding effect that unifies Li^+ flux and promotes homogeneous Li plating.

Most studies tried to improve the cycling performance of Li–S batteries with modifications only concentrated on the cathode or the anode. Since the S cathode and Li anode are not stable in Li–S batteries, there should be a holistic consideration. Herein, a PIL is synthesized. It is applied in both the cathode and anode to improve the cycling performance of Li–S batteries. The cross-linked PIL shows a strong adsorption capacity for polysulfides, which can inhibit their dissolution and shuttling. The PIL film on the Li anode surface can homogenize Li^+ flux and promote large size Li deposition. The Li–S battery modified by the PIL at the anode and cathode shows much improved cycling stability and C-rate performance.

2 Experimental section

2.1 Synthesizing poly(ionic liquid) (PIL)

2.1.1 Synthesizing ionic liquid (IL-CN-Br). Bromoacetonitrile (3.0 g) and 1-vinylimidazole (2.0 g) were dissolved in 25.0 mL tetrahydrofuran (THF). The reaction was carried out for 10 h at 60 °C under a N_2-filled flask, followed by cooling the precipitates to room temperature. Subsequently, the precipitates were subjected to high-speed centrifugation to collect the white product. After three repeated washings with THF to remove any unreacted monomers, the product was dried at 60 °C in a vacuum oven for 12 h to obtain the desired monomer IL-CN-Br. (Yield: ~80%).

2.1.2 Preparing poly(ionic liquid) (PIL-Br). 2.0 g IL-CN-Br monomer was dissolved in 19.0 mL dimethyl sulfoxide (DMSO) with stirring under a N_2-filled flask for at least 1 h. Then, 16.0 mg 2,2′-azobis(2-methylpropionitrile), dissolved in 1.0 mL DMSO, was injected using a syringe, and the reaction mixture was heated at 80 °C for 48 h. After that, the solution was added dropwise to THF (200.0 mL). The precipitate was collected, and washed three times with THF. Finally, the product was dried at 60 °C for 24 h to obtain PIL-Br.

2.1.3 Preparing poly(ionic liquid) with bis(trifluoromethane)-sulfonimide (PIL). PIL was prepared by ion exchange. Two solutions were prepared first. *A solution*: 1.4 g (4.88 mmol) bis(trifluoromethane)sulfonimide lithium salt (LiTFSI) was dissolved in 1.0 mL deionized water at room temperature. *B solution*: 0.60 g (2.80 mmol) PIL-Br was dissolved in 30.0 mL deionized water. *A solution* was introduced into the *B solution* and stirred at 600 rpm. After that, the yellow flocculent precipitate was obtained through counter ion exchange. Afterwards, it was washed three times with deionized water and dried under vacuum at 60 °C for 24 h to obtain PIL. The PIL has bis(trifluoromethane)sulfonimide as anions.

2.1.4 Preparing cross-linked poly(ionic liquid) (c-PIL). 0.10 g PIL was dissolved in 1.0 mL dimethyl formamide (DMF), and then carefully dropped onto a clean Petri dish before being placed in NH_3-filled atmosphere for 12 h, during which the PIL was cross-linked to form c-PIL. After that, the c-PIL film was immersed in deionized water to peel off from the dish's surface. Finally, the obtained c-PIL film was further dried at 60 °C.

2.2 Electrode preparation and battery assembly

2.2.1 c-PIL@S cathode and blank S cathode. Sublimed sulfur (Shanghai Aladdin Bio-Chem Technology Co., Ltd) was mixed with CNTs (FT9000, Jiangsu Cnano Technology Co., Ltd) with a mass ratio of 7 : 3. The mixtures were then sealed in a reactor container and heated at 155 °C for 20 h to make sulfur and CNTs disperse fully to obtain the S/CNTs composite. The c-PIL@S cathode slurry was prepared by mixing 80.0 wt% S/CNTs, 10.0 wt% Super P, 5.0 wt% PIL and 5.0 wt% PVDF binder in NMP solvent. The slurry was cross-linked under NH_3 atmosphere for 24 h, uniformly coated onto carbon-coated Al foil and then dried under vacuum at 60 °C for 24 h to obtain c-PIL@S composite cathode (Fig. S1, ESI†). Blank S cathode slurry was prepared by mixing 80.0 wt%, S/CNTs, 10.0 wt% Super P and 10.0 wt% PVDF binder in NMP solvent. The slurry was coated onto carbon coated Al foil and dried under vacuum at 60 °C for 24 h. The sulfur content in the c-PIL@S cathode and S cathode was about 59% (Fig. S2, ESI†). The sulfur loading of the prepared c-PIL@S cathode was about 1.0 mg cm^{-2}.

Open Access Article. Published on 07 March 2024. Downloaded on 2/7/2026 9:32:35 PM. This article is licensed under a Creative Commons Attribution-NonCommercial 3.0 Unported Licence.

2.2.2 PIL@Li anode and PIL@Cu electrode. The PIL polymer was dissolved in dry DMSO to obtain a 5.0 wt% polymer solution, which was then spin-coated onto a commercial lithium foil in a dry room (temperature: 19.5 °C, dew point: < -40 °C). The PIL coated Li foils were vacuum dried in an oven at 60 °C for 5 h to obtain the PIL@Li anode. The PIL@Cu electrode was prepared by the same method as above. The thickness of the PIL artificial SEI layer is about 2 μm (Fig. S3, ESI†).

2.2.3 Battery assembly. PIL@Li‖c-PIL@S and Li‖S batteries were assembled. On the surface of the cathode, 15.0 μL LE was dropped first. Then a 16 μm PE separator was laid on with another 15.0 μL LE. After that, the Li anode (∅: 15.6 mm, *l*: 0.45 mm), stainless steel plate and spring sheet were put on sequentially, and sealed. The LE was comprised of 1.0 M LiTFSI in DOL/DME (1 : 1 v/v) with 1.0 wt% $LiNO_3$. The electrolyte/sulfur (E/S) ratio was about 38.22 μL mg^{-1}. The identical procedure and materials were employed for the preparation of Li‖Li battery, PIL@Li‖Li@PIL battery and Li‖Cu battery, Li‖PIL@Cu battery. All procedures were carried out in an Ar-filled glove box.

2.3 Preparing Li_2S_6 solution

In the glove box, 0.8 g S powder and 0.23 g Li_2S powder (the molar ratio between S and Li_2S is 5 : 1) were added to 10 mL DME/DOL (the volume ratio between DME and DOL is 1 : 1). Under the Ar atmosphere, the mixture was placed in an oil bath at 80 °C and stirred for 6 h to prepare 0.5 mol L^{-1} purple-black Li_2S_6 solution. The test solution has been diluted in order not to exceed the detection limit of the instrument.

2.4 Material characterization

The structure of IL-CN-Br and PIL-Br was characterized by ^{1}H NMR (JNM-ECZ600R). The Fourier-transform infrared (FTIR) spectrum was recorded using SHIMADZU IRAffinity-1 in the range from 4000 to 400 cm^{-1} to investigate the chemical structure of samples. X-ray photoelectron spectroscopy (XPS) test was explored on the ESCALab 250Xi (Thermo Fisher Scientific). The surface of Li deposition layer was characterized after the PIL layer was removed. The UV-vis spectra were performed with a Cary 60 UV-vis spectrometer (Agilent Technologies). The morphology of samples was characterized by a field-emission scanning electron microscopy (SEM, SU-8010, Hitachi) and a transmission electron microscope (TEM, Talos F200S, Thermo Fisher Scientific). The thermogravimetric analysis of c-PIL was measured by an apparatus (Q600 SDT America, TA Instruments) from 25 °C to 800 °C.

2.5 Density functional theory (DFT) calculation

The molecular orbital energy and binding energy calculations were operated under the framework of DFT with B3LYP functional and 6-31+G(d,p) basis set. All calculations were performed using the Gaussian 09 program. The binding energy (E_b) was calculated as $E_b = E_{c\text{-}PIL/Li_2S_6} - E_{c\text{-}PIL} - E_{Li_2S_6}$, where $E_{c\text{-}PIL/Li_2S_6}$ is the energy of the interaction system for Li_2S_6 with c-PIL, $E_{c\text{-}PIL}$ and $E_{Li_2S_6}$ are the energies of Li_2S_6 and c-PIL molecules, respectively.

2.6 Electrochemical characterization

The galvanostatic discharge/charge cycling performance of batteries was evaluated using the LAND testing system (LANHE CT2001A). An electrochemical workstation (interface 1000E, Gamry Instruments) was used to characterize the electrochemical performance. Electrochemical impedance spectra (EIS) were tested in the frequency range of 10^6 to 10^{-1} Hz. The CV was scanned in the voltage range of 1.8 to 2.8 V at a scanning rate of 0.01 mV s^{-1}. The apparent chemical diffusion coefficient of Li ion (D_{Li^+}) can be calculated by the Randles–Sevick equation.[40,41]

$$I_p = 2.69 \times 10^5 n^{3/2} C_{Li^+} A D_{Li^+}{}^{1/2} \nu^{1/2}$$

where I_p is the peak current, n is the charge transfer number, A is the surface area of the electrode, C_{Li^+} is the Li ion concentration in unit volume, and v is the scan rate.

3 Results and discussion

Imidazole-based PIL was synthesized, and it was further cross-linked with the triazine ring using a mild and straightforward method.[42,43] The detailed synthesis procedures are shown in Fig. S4 (ESI†). The ^{1}H NMR verifies the polymerization of vinylimidazole (Fig. S5a and b, ESI†). c-PIL was obtained by ammonia vapor treatment, during which the nitrile groups reacted. The formation of triazine is verified in IR and XPS spectra (Fig. S6a and b, ESI†). c-PIL has high thermal stability with a degradation temperature higher than 300 °C (Fig. S7, ESI†). Furthermore, when ignited with liquid electrolyte, it shows self-extinguishing properties (Fig. S8, ESI†). These characteristics are extremely precious for the safety of Li–S batteries.

The "shuttle effect" of LiPS in Li–S batteries is considered to be one of the major factors affecting long-term cycling performance. The PIL with IL moieties on the side is able to generate strong van der Waals and electrostatic interactions,[20,44,45] so the binding energy (E_b) between PIL and Li_2S_6 was calculated to evaluate the adsorption of polysulfides. For simplicity, the configuration of c-PIL was modified with one imidazole unit attached to the triazine ring (Fig. S9, ESI†). As shown in Fig. 1a, the E_b between simplified c-PIL and Li_2S_6 is −2.094 eV, much lower than that between PIL and Li_2S_6 (−1.075 eV). The E_b between c-PIL and Li_2S_6 will further decrease, since there are more sites to associate with Li_2S_6. Lower E_b suggests that there is stronger van der Waals and electrostatic interaction between c-PIL and Li_2S_6. This indicates that the adsorption capability of PIL on Li_2S_6 can be further strengthened with c-PIL by cross-linking with triazine. The insert in Fig. 1b demonstrates that when PIL mixes with the polysulfide solution, the color of the solution changes from dark brown to bright yellow after 10 hours. Whereas the color becomes almost colorless in the c-PIL containing solution, indicating a substantial decrease in polysulfide concentration due to the adsorption by c-PIL.

© 2024 The Author(s). Published by the Royal Society of Chemistry

Open Access Article. Published on 07 March 2024. Downloaded on 2/7/2026 9:32:35 PM.
This article is licensed under a Creative Commons Attribution-NonCommercial 3.0 Unported Licence.

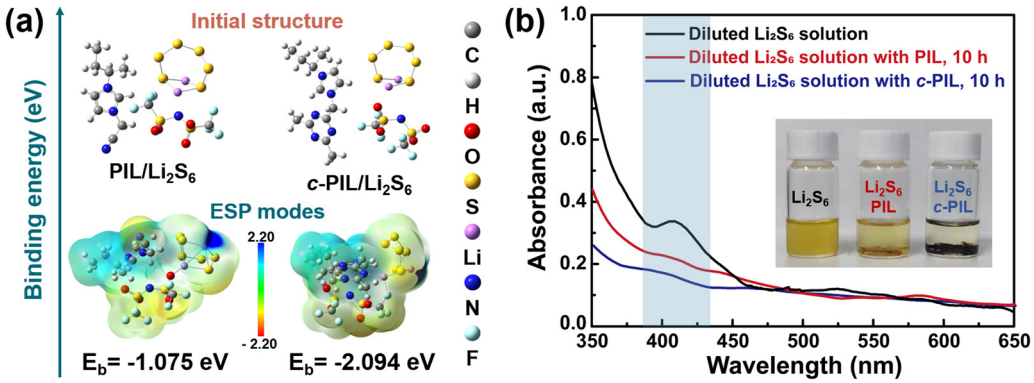

Fig. 1 (a) The binding energies, initial structures and the optimized electrostatic potential surfaces of polysulfide to PIL and c-PIL. (b) The UV-vis spectra of polysulfide adsorption tests with PIL and c-PIL. The insertion showing the photographs of diluted Li_2S_6 solutions.

In UV-vis spectroscopy, the characteristic peaks around 350–450 nm can be attributed to polysulfides.[46,47] As shown in Fig. 1b, for the c-PIL containing solution, the absorption intensity at 350–450 nm decreases greatly after 10 h, much lower than that of the fresh polysulfide solution. The results are consistent with E_b calculation and the observed color evolution, consolidating the strong adsorption capacity of c-PIL. In order to investigate whether the adsorption/desorption is reversible in the electrolyte, UV-vis spectroscopy was measured for the mixture of liquid electrolyte and the polysulfide-absorbed c-PIL (Fig. S10, ESI†). The peaks at 350–450 nm, attributed to polysulfides, are observed in the mixture, verifying that the absorbed polysulfide can be released and reversibly exchanged with the anion groups ($TFSI^-$) in liquid electrolyte.[23] The results demonstrate that c-PIL can be used as a new absorbent for LiPSs to confine them in the cathode and effectively decrease their concentration in liquid electrolyte, which is beneficial for stabilizing the cathode structure and improving the utilization efficiency of the active substance.

CV curve of the c-PIL@S cathode shows that two reduction peaks appear at higher potentials and two oxidation peaks start at lower potentials than those of ordinary S cathode (Fig. S11, ESI†). Smaller polarization observed in the c-PIL@S cathode (275 mV) than in the ordinary S cathode (338 mV) indicates that smaller overpotential is needed for the reaction, which means that the reduction and oxidation reactions take place easier with the presence of c-PIL. It is deduced that c-PIL may act as a catalyzer to change the energy barrier of the conversion reaction of polysulfides. No other peaks are seen in the CV profiles, suggesting that c-PIL is electrochemically stable in the scan voltage range, and doesn't bring extra side reactions to the cathode.

PIL was further used as an artificial SEI layer on the Li metal anode to counteract the growth of lithium dendrites and the formation of "dead lithium". Li‖PIL@Cu cells were assembled. After the 1st discharge cycle, the morphology of Li deposition on PIL coated Cu foil was observed with SEM. As shown in Fig. 2a–c, the PIL coating is flat and featureless, and Li is plated between PIL and Cu foil. When Li is deposited at 0.1 mA h cm^{-2}, the deposited Li is barely discernible on the exposed area (Fig. 2a). In contrast, some small spherical Li depositions appear on the surface of Cu foil from Li‖Cu cells (Fig. 2d). So, it is supposed that the PIL coating may have consumed the deposited Li. To investigate how much capacity will be consumed, the initial several discharged profiles of Li‖PIL@Cu cells discharged to 0 V are displayed. As shown in Fig. S12 (ESI†), several discharge platforms appear in the first cycle, and about 0.09 mA h is discharged. In the subsequent cycles, the discharge platforms disappear. It means that the first discharge capacity is not reversible, and the active Li has been consumed by the reaction with PIL. Although the reaction will decrease the initial Coulombic efficiency (CE) of Li‖PIL@Cu, it may promote the formation of a stable interface layer on freshly deposited Li.[48,49] As Li is plated at 0.5 mA h cm^{-2}, sporadic spherical Li deposition with the size of about 3.0 μm is observed below the PIL coating (Fig. 2b). Whereas different morphology is seen on Cu foil from Li‖Cu cells (Fig. 2e). Tightly packed spherical Li deposition with the size of 1.5 μm forms on the bottom with Li dendrites on the upper layer. As Li is plated at 1.0 mA h cm^{-2}, dendrite-free Li deposition is observed below the PIL coating, while proliferated Li dendrites are seen on Cu foil (Fig. 2c and f). From the large size and dendrite-free Li deposition, it can be concluded that the PIL coating have modified the Li deposition behavior. Huang *et al.*[39] concluded that PIL on Li foil can tailor Li deposition behavior by homogenizing the Li^+ flux through electrostatic shielding, which should have played a vital role in promoting uniform Li deposition. Besides, the reaction with PIL during the first cycle may also have a significant impact.

Density function theory (DFT) calculation was further carried out to investigate the possible contribution of the reaction in the first cycle. The highest occupied molecular orbital (HOMO) and lowest unoccupied molecular orbital (LUMO) levels of the components in the liquid electrolyte (DME, DOL, LiTFSI) and PIL were calculated. As showed Fig. 3, PIL exhibits a significantly lower LUMO energy (−2.84 eV) compared to the solvents (−0.18 and −0.24 eV for DME and DOL) and LiTFSI (−1.47 eV). Generally, materials with a lower LUMO energy facilitate electron acceptance and can be reduced first.[50,51] Hence, the capacity loss in the first cycle shall originate from the reduction of PIL. The surface potential distribution shows

Open Access Article. Published on 07 March 2024. Downloaded on 2/7/2026 9:32:35 PM.
This article is licensed under a Creative Commons Attribution-NonCommercial 3.0 Unported Licence.

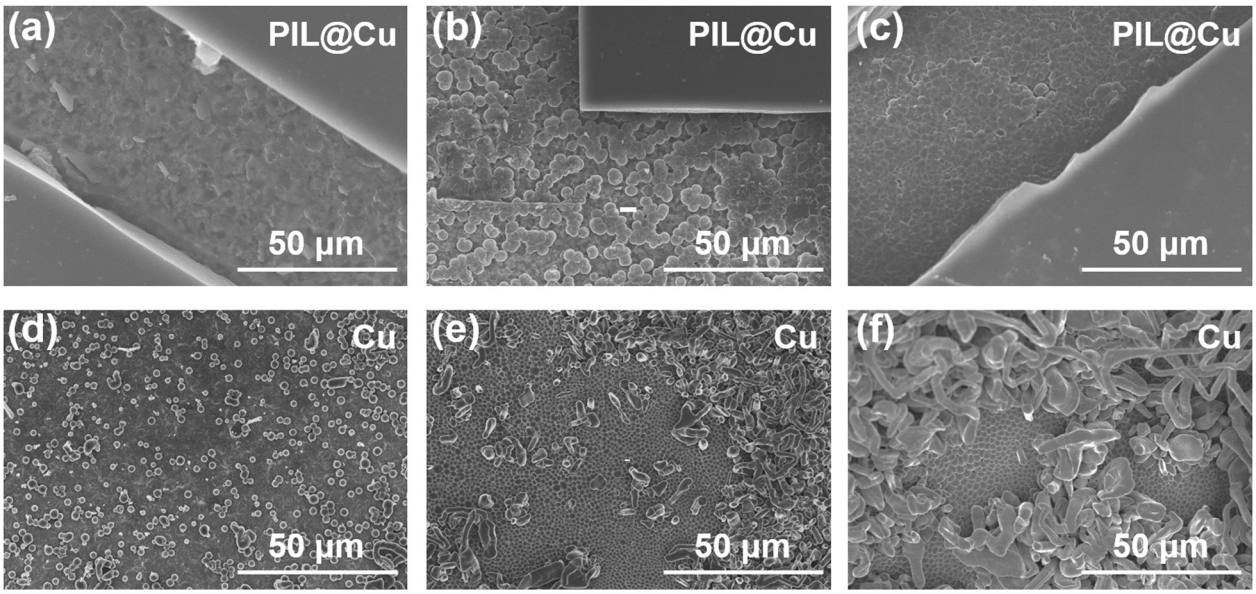

Fig. 2 SEM images of Li deposition morphology. Li deposited on PIL@Cu foil at (a) 0.1 mA h cm^{-2}, (b) 0.5 mA h cm^{-2} and (c) 1.0 mA h cm^{-2}. Li deposited on Cu foil at (d) 0.1 mA h cm^{-2}, (e) 0.5 mA h cm^{-2} and (f) 1.0 mA h cm^{-2}.

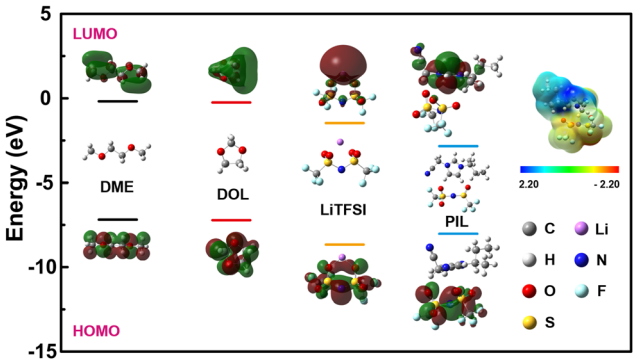

Fig. 3 DFT calculation on the HOMO and LUMO energies of DME, DOL, LiTFSI and PIL, the electrostatic potential charge distribution of PIL.

that the imidazole exhibits a strong positive charge, indicating that the imidazole is easily reduced.

XPS tests were conducted on the PIL removed PIL@Cu foil before and after Li deposition. In the Li 1s profiles, it can be observed that the characteristic peaks for Li_3N (55.0 eV) and LiF (55.7 eV) appear on the original Li free surface after Li deposition[52,53] (Fig. S13a and b, ESI†). In the N 1s profiles, the peak at 398.9 eV can also verify the formation of Li_3N after Li deposition[54,55] (Fig. S13c and d, ESI†). From DFT calculation and XPS results, it can be deduced that the N contained imidazole in PIL has been reduced by active Li to form Li_3N rich layer on the interface. Li_3N is a good ionic conductor for Li^+ and can act as lithiophilic nucleus to induce uniform Li deposition.[54,56] Therefore, it is supposed that the Li_3N rich interfacial layer should have promoted the dendrite-free Li deposition beneath the PIL coating layer (Fig. 2b and c).

Dendrite-free Li deposition with reduced specific surface can slow the reaction of the liquid electrolyte with freshly deposited Li, which is helpful for improving the CE of Li‖Cu cells. It can be seen that the Li‖PIL@Cu cells can stably run for more than 200 cycles with the CE of 98.6% and 98.2% at current densities of 0.2 and 0.5 mA cm^{-2}, respectively (Fig. 4a). Even at the current density of 1.0 mA cm^{-2}, it can stably run for 158 cycles with the CE of 96.6%. While the Li‖Cu cells can only stably run for 123, 77 and 24 cycles (Fig. 4b). The improved cycling stability of Li‖PIL@Cu cells may first benefit from the dendrite-free Li deposition below the PIL coating layer on Cu foil. Moreover, the physical isolation role of the PIL coating layer should not be neglected. As shown in Fig. S14a (ESI†), when Li is plated, the surface is covered with a featureless PIL coating, which can alleviate the reaction of freshly deposited Li with liquid electrolyte (Fig. S14b, ESI†). The role of the PIL coating layer in stabilizing the interface of Li deposition can also be observed from the polarization voltages evolution. As shown in Fig. 4c, although the Li‖PIL@Cu cell has higher polarization (174 mV) than that of the Li‖Cu cell (34 mV) in the first cycle due to the lower ionic conductivity, it decreases to 23 mV after 100 cycles, in contrast to 66 mV in the Li‖Cu cell (Fig. 4d). Large polarization increases in the Li‖Cu cell means the continuous reaction of liquid electrolyte with freshly deposited Li, resulting in heavy accumulation of SEI film and "dead Li".[57] As a comparison, small polarization observed in the Li‖PIL@Cu cell suggests stable Li deposition interface has been constructed with the help of PIL coating layer, which is beneficial for improving CE.

Symmetric cells were assembled to further evaluate the role of the PIL coating layer. It can be observed that the Li@PIL‖PIL@Li cells can stably run for more than 2000 h, much longer than that of the Li‖Li symmetric cells at various current densities (Fig. S15a–c, ESI†). The morphology of the Li electrode shows that the PIL coating layer is still uniform after

© 2024 The Author(s). Published by the Royal Society of Chemistry

Open Access Article. Published on 07 March 2024. Downloaded on 2/7/2026 9:32:35 PM.
This article is licensed under a Creative Commons Attribution-NonCommercial 3.0 Unported Licence.

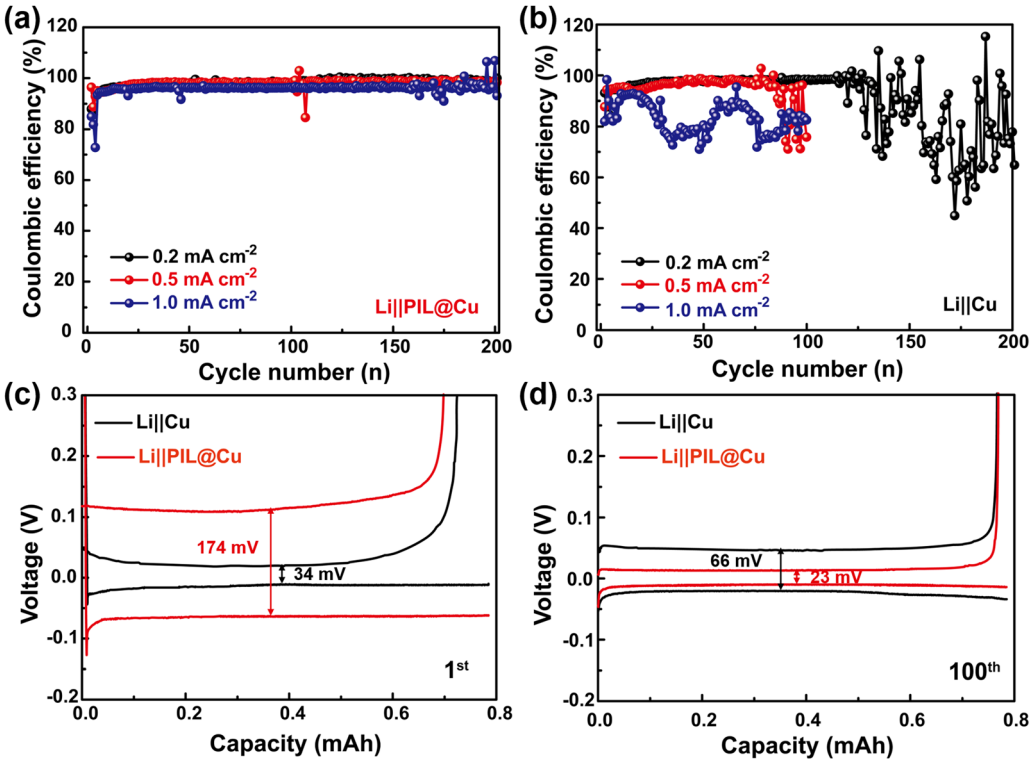

Fig. 4 Coulombic efficiency of (a) Li‖PIL@Cu and (b) Li‖Cu batteries at 1.0 mA h cm^{-2}. Discharge and charge curves of Li‖PIL@Cu and Li‖Cu batteries in the (c) 1st and (d) 100th cycle at 0.2 mA cm^{-2} and 1.0 mA h cm^{-2}.

100 cycles and no cracks or Li dendrites are seen on the PIL@Li (Fig. S16a, ESI†). While pulverized morphology is observed on the Li electrode (Fig. S16b, ESI†). The results further confirm the protection role of the PIL coating layer on Li electrode by alleviating the corrosion of LE, homogenizing the electric field and promoting uniform Li deposition.

c-PIL modified cathode and PIL coated Li anode were used to assemble PIL@Li‖c-PIL@S battery. The galvanostatic charge/discharge profiles of the Li–S batteries are shown in Fig. 5a. Two discharge plateaus are observed, which can be attributed to the formation of Li_2S_x (x = 4–8) and Li_2S_y (y = 1–2), respectively.[58,59] The discharge plateaus of the PIL@Li‖c-PIL@S battery is slightly lower than that of the Li‖S battery, indicating that activation is needed for the PIL coating layer. The PIL@Li‖c-PIL@S battery has longer discharge plateaus and shows higher initial discharge capacities, indicating that modification of S cathode with c-PIL is effective in slowing down the loss of active materials. The cycling performances of the Li–S batteries are shown in Fig. 5b and Fig. S17 (ESI†). Fig. S17 (ESI†) shows that 5 wt% content of the c-PIL is a more appropriate proportion to improve the cycling performance of Li–S batteries. In Fig. 5b, the capacity of PIL@Li‖S battery decays as fast as that of the Li‖S battery in the first 50 cycles, meaning that modification only on the anode can't inhibit the loss of active material. After 50 cycles, the capacity decays in a much slower rate, demonstrating that the PIL artificial SEI layer can stabilize the interface on the Li anode. The Li‖c-PIL@S battery has much higher capacity than that of the Li‖S battery, verifying that the active material is well confined in the cathode by c-PIL. However, after 150 cycles, the capacity of Li‖c-PIL@S battery decays at the same rate as that of Li‖S battery. The results imply that the faster capacity decay may originate from the un-protected Li, which may have resulted in the exhaustion of liquid electrolyte.[60,61] It can be concluded that modification on the S cathode can alleviate capacity loss in the early stage, while protecting Li anode can prevent the capacity diving in the later stage. Therefore, simultaneously modifying the S cathode and Li anode can further improve the cycling performance of Li–S batteries. The discharge capacity retention ratio of the PIL@Li‖c-PIL@S battery is 68.7% after 300 cycles, which is significantly higher than that of the Li‖S battery (42.0%). The results corroborate that our strategy of modifying the S cathode with c-PIL and protecting the Li anode with PIL is effective in improving the long-term cycling performance compared with those reported in the literature (Table S1, ESI†).

XPS was used to characterize the PIL removed Li deposition surface from the disassembled batteries. As shown in Fig. 5c–f, the S 2p doublet spectra are observed due to the closely spaced $2p_{3/2}$ and $2p_{1/2}$ spin-orbits.[62,63] The strong peaks at 169.4 and 167.4 eV are attributed to SO_4^{2-} and SO_3^{2-} or $S_2O_3^{2-}$ species derived from the decomposition products of LiTFSI, respectively.[64,65] Besides, the broad peaks at 160–165 eV refer to sulfides with chemical valence between −2 to 0, which originate from the reduction of "shuttled polysulfides" on the Li anode. Thereinto, the two peaks at 162.8 and 164.1 eV are assigned to the terminal sulfur (S_T^{1-}) and bridging sulfur (S_B^0),

Open Access Article. Published on 07 March 2024. Downloaded on 2/7/2026 9:32:35 PM.
This article is licensed under a Creative Commons Attribution-NonCommercial 3.0 Unported Licence.

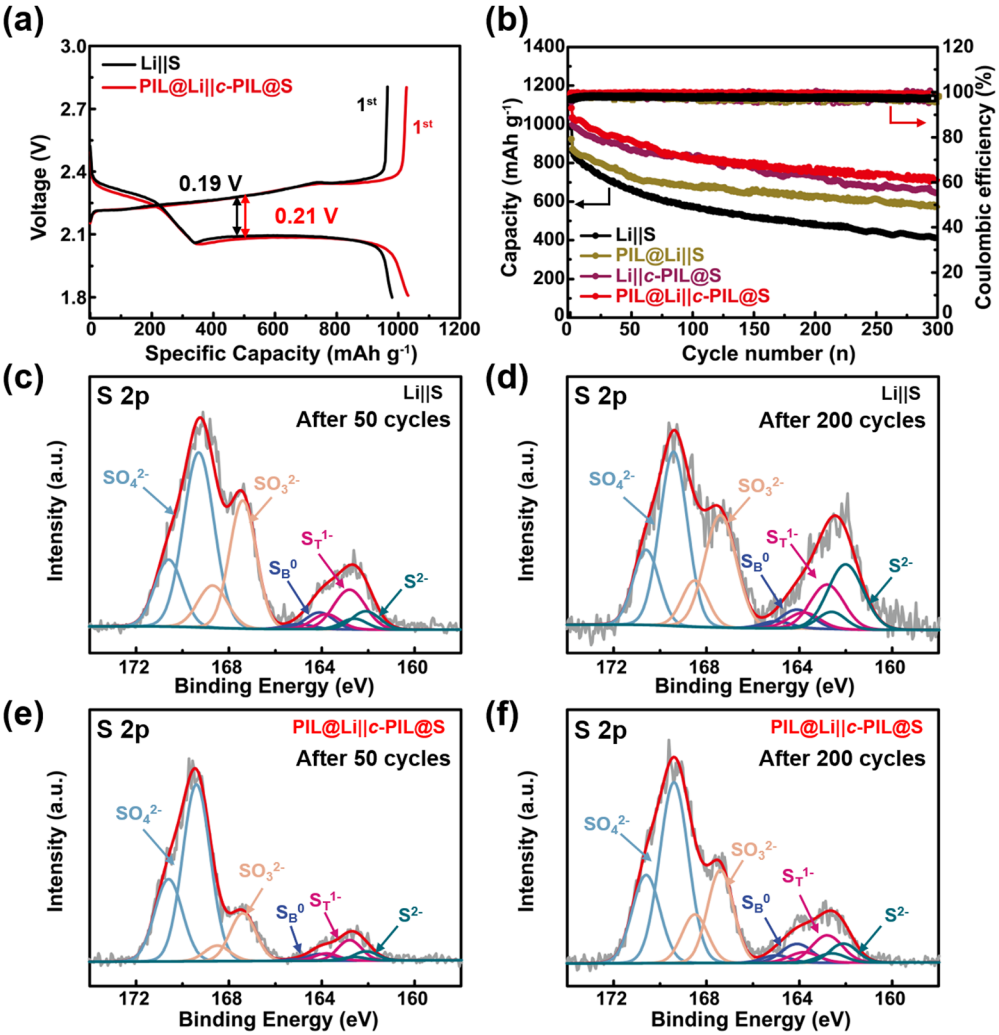

Fig. 5 (a) The discharge/charge profiles of PIL@Li‖c-PIL@S and Li‖S batteries at the first cycle of 0.5C. (b) The cycling performance at 0.5C of the PIL@Li‖c-PIL@S and Li‖S batteries. The XPS spectra of S 2p on lithium anode after different cycles in (c) and (d) Li‖S and (e) and (f) PIL@Li‖c-PIL@S batteries.

and the peak at 162.1 eV belongs to reduced sulfur species (S^{2-}).[66,67] The profiles are normalized with the original data at about 169.4 eV. The intensity of the peak at 167.4 eV is much higher in Fig. 5c than that in Fig. 5e after 50 cycles. After 200 cycles, these trends still exist (Fig. 6d and f). It suggests that the decomposition of LiTFSI and the reduction of polysulfides on the Li anode are greatly decreased with the protection of the PIL coating layer. Higher intensity of the peak at 162.1 eV (Fig. 5c and d *vs.* Fig. 5e and f) means the formation of more insoluble insulated Li_2S on the Li anode in Li‖S batteries, which may lead to obvious increase in internal resistance during cycling. The EIS tests were used to monitor the internal resistance evolution. As shown in Fig. S18 and Table S1 (ESI†), although the solid electrolyte interphase impedance (R_{SEI}) and charge transfer impedance (R_{ct}) are less in Li‖S battery in the 1st cycle (Fig. S18a, ESI†), they are much larger than those in PIL@Li‖c-PIL@S battery after 100 cycles (Fig. S18b, ESI†). The smaller R_{SEI} after 100 cycles suggests that more stable SEI layers are constructed, and Li^+ transports more easily at the interface of the anode. The shuttling of polysulfides and the formation of insulated Li_2S on the Li anode have been greatly inhibited. SEM images of blank S and c-PIL@S cathodes are shown in Fig. S19 (ESI†). Porous structure is observed on both cathodes in Fig. S19a and c (ESI†). After 50 cycles, minor changes can be seen on the c-PIL@S cathode (Fig. S19b, ESI†), while some merged morphologies are observed on the blank S cathode (Fig. S19d, ESI†). The merged morphologies indicate that insoluble Li_2S and Li_2S_2 accumulate on the surface due to the shuttling of polysulfides.

The C-rate performance is shown in Fig. 6a. It can be observed that the PIL@Li‖c-PIL@S battery delivers much higher capacities than that of the Li‖S battery at all C-rates. As the rate is returned to 0.1C, a much higher capacity recovery indicates highly reversible electrochemistry and much better redox kinetics. To investigate whether the modification on the S cathode with c-PIL can promote the reaction kinetics, CV curves were scanned at variable rates (0.1–2.0 mV s^{-1}) as shown in Fig. 6b and c. It can be seen that the PIL@Li‖c-PIL@S battery

© 2024 The Author(s). Published by the Royal Society of Chemistry

Open Access Article. Published on 07 March 2024. Downloaded on 2/7/2026 9:32:35 PM.
This article is licensed under a Creative Commons Attribution-NonCommercial 3.0 Unported Licence.

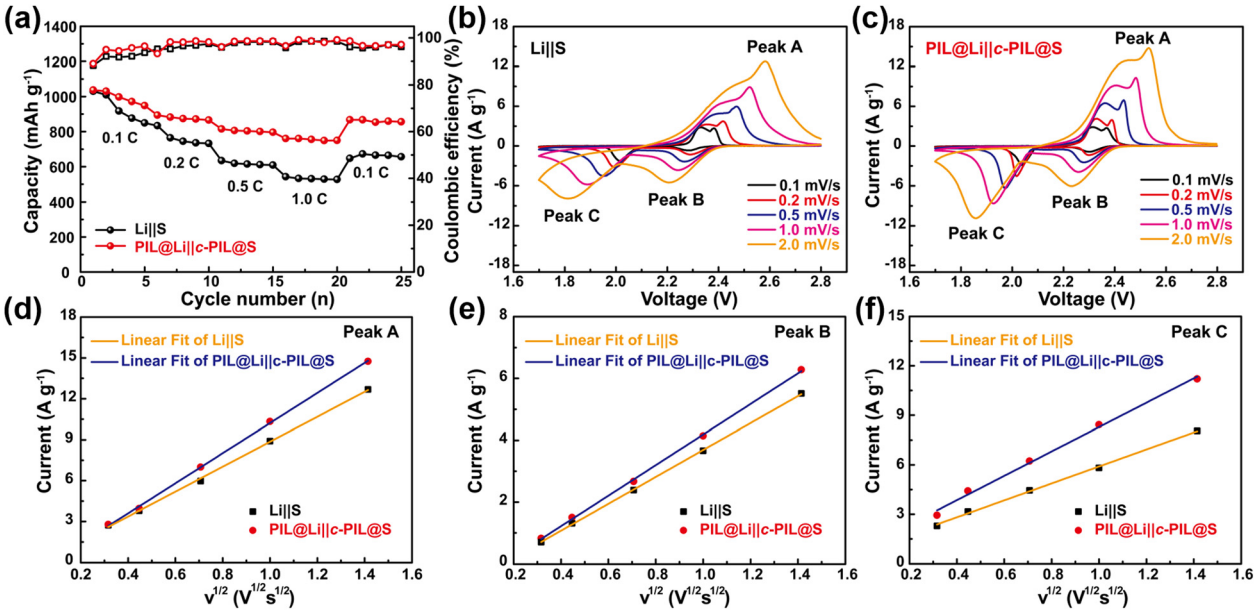

Fig. 6 (a) C-rate performance of the PIL@Li‖c-PIL@S and Li‖S batteries. The CV profiles of (b) Li‖S and (c) PIL@Li‖c-PIL@S batteries at varied scanning rates from 0.1 to 2.0 mV s^{-1}. (d)–(f) Linear fitting of peak current and the square root of scanning rate in PIL@Li‖c-PIL@S and Li‖S batteries.

shows a higher peak current and a larger CV area than Li‖S battery at all scan rates, indicating that the reaction kinetics and sulfur utilization have been improved a lot with the aid of c-PIL. The peak currents exhibit a linear correlation with the square root of the scan rate (Fig. 6d–f), so both the oxidation and reduction processes are controlled by diffusion. Therefore, the slope of the fitting line could be applied to further evaluate the diffusion coefficient (D_{Li^+}) in S cathodes according to the Randles–Sevick equation.[68,69] For the PIL@Li‖c-PIL@S and Li‖S batteries, the slopes of fitting lines are 11.04 and 9.15 for peak A, 4.95 and 4.36 for peak B, 7.39 and 5.15 for peak C, respectively. From the slopes, D_{Li^+} ratio can be calculated to be 1.21, 1.14 and 1.43, suggesting that Li migrates much faster in the c-PIL@S cathode. Therefore, it is supposed that when c-PIL is used, the hanged IL groups have promoted Li^+ diffusion in the S cathode as well as reaction kinetics.

Fig. 7 schematically illustrates multiple roles of the PIL in Li–S batteries. In the cathode, the triazine cross-linked c-PIL has strong adsorption on polysulfides, which confines the polysulfides in the S cathode and inhibits the shuttling of LiPSs. The IL moieties hanged on the main chain of c-PIL has promoted the diffusion of Li^+ and enhanced the reaction kinetics. On the anode, PIL, as an artificial SEI layer, can isolate the liquid electrolyte from deposited Li, stabilize the interface of Li foil and promote uniform Li deposition beneath the coating layer. Cycling performance of Li–S batteries has been improved by functionalizing the S cathode and Li metal anode with PIL.

4 Conclusions

PIL was synthesized to modify the S cathode and Li metal anode in Li–S batteries. The triazine cross-linked c-PIL has a much stronger adsorption capacity for polysulfides. DFT calculations show that the binding energy between c-PIL and Li_2S_6 is very negative, verifying that the strong van der Waals and electrostatic interactions promote the adsorption of polysulfides. The c-PIL modified S cathode can confine the polysulfides by adsorption and effectively inhibit the shuttling of LiPS. Furthermore, Li^+ diffusion coefficient can be improved by c-PIL modification in the S cathode. PIL as an artificial SEI layer on the Li metal anode can homogenize the Li^+ flux and promote

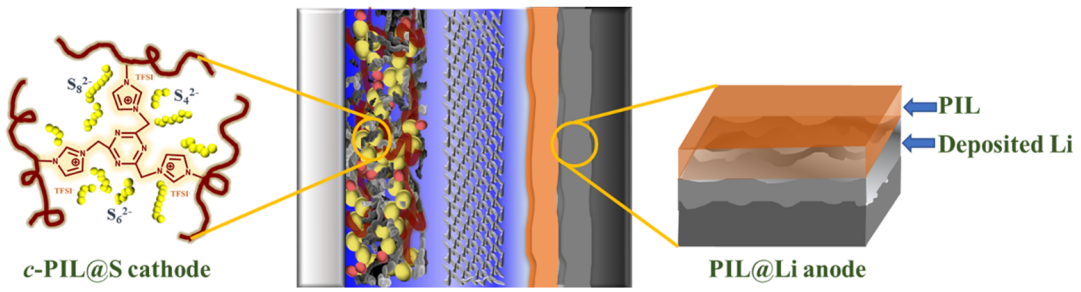

Fig. 7 Schematic diagram of a Li–S battery with improved cycling performance by functionalizing S cathode and Li anode with PIL.

Open Access Article. Published on 07 March 2024. Downloaded on 2/7/2026 9:32:35 PM. This article is licensed under a Creative Commons Attribution-NonCommercial 3.0 Unported Licence.

uniform Li deposition. DFT and XPS results show that the N containing imidazole in PIL can be reduced by active Li to form a Li_3N rich layer on the interface. The Li_3N containing interfacial layer promoted the dendrite free Li deposition beneath the PIL coating layer. Li–S batteries with the c-PIL modified cathode and PIL coated Li anode show significant improvements in cycling stability and C-rate performance.

Author contributions

Sixin Jia: formal analysis, writing – original draft, software, and visualization. Rui Wang: data curation, and investigation. Fengquan Liu: validation and methodology. Hong Huo: project administration and resources. Jianjun Zhou: writing – review & editing, methodology, and conceptualization. Lin Li: writing – review & editing and funding acquisition.

Conflicts of interest

There are no conflicts of interest to declare.

Acknowledgements

The authors appreciate the support from the Natural Science Foundation of China (Grant No. 22179010, 21973008, and 22109079)

Notes and references

1 H. Pan, Z. B. Cheng, Z. Y. Zhou, S. J. Xie, W. Zhang, N. Han, W. Guo, J. Fransaer, J. S. Luo, A. Cabot and M. Wübbenhorst, *Nano-Micro Lett.*, 2023, **15**, 165.
2 P. G. Bruce, S. A. Freunberger, L. J. Hardwick and J. M. Tarascon, *Nat. Mater.*, 2011, **11**, 19–29.
3 H. J. Peng, J. Q. Huang, X. B. Cheng and Q. Zhang, *Adv. Energy Mater.*, 2017, **7**, 1700260.
4 A. Manthiram, Y. Z. Fu, S. H. Chung, C. X. Zu and Y. S. Su, *Chem. Rev.*, 2014, **114**, 11751–11787.
5 X. L. Ji, K. T. Lee and L. F. Nazar, *Nat. Mater.*, 2009, **8**, 500–506.
6 J. N. Wang, H. L. Wang, S. Y. Jia, Q. Zhao, Q. Zheng, Y. L. Ma, T. Y. Ma and X. Li, *J. Energy Storage*, 2023, **72**, 108372.
7 Z. Y. Chi, J. L. Ding, C. Ding, B. W. Cui, W. Q. Wang and G. C. Wang, *ACS Appl. Mater. Interfaces*, 2023, **15**, 39342–39350.
8 H. Raza, S. Y. Bai, J. Y. Cheng, S. Majumder, H. Zhu, Q. Liu, G. P. Zheng, X. F. Li and G. H. Chen, *Electrochem. Energy Rev.*, 2023, **6**, 29.
9 D. C. Lin, Y. Y. Liu and Y. Cui, *Nat. Nanotechnol.*, 2017, **12**, 194–206.
10 N. W. Li, Y. X. Yin, J. Y. Li, C. H. Zhang and Y. G. Guo, *Adv. Sci.*, 2017, **4**, 1600400.
11 Z. Huang, L. J. Wang, Y. Y. Xu, L. F. Fang, H. Li, B. K. Zhu and Y. Z. Song, *Chem. Eng. J.*, 2022, **443**, 136347.
12 T. Guo, Y. C. Ding, C. Xu, W. X. Bai, S. C. Pan, M. L. Liu, M. Bi, J. W. Sun, X. P. Ouyang, X. Wang, Y. S. Fu and J. W. Zhu, *Adv. Sci.*, 2023, e2302518.
13 X. G. Zhang, Y. Yang, Y. Y. Wu, X. Xu and Z. J. Huang, *J. Environ. Chem. Eng.*, 2023, **11**, 110683.
14 A. Dzieniszewska, J. Nowicki, G. Rzepa, J. Kyziol-Komosinska, I. Semeniuk, D. Kielkiewicz and J. Czupiol, *Int. J. Biol. Macromol.*, 2022, **210**, 483–493.
15 I. A. Lawal, M. Klink, P. Ndungu and B. Moodley, *Environ. Res.*, 2019, **175**, 34–51.
16 H. Musarurwa and N. T. Tavengwa, *Sustainable Chem. Pharm.*, 2021, **24**, 100545.
17 J. Y. Yuan, D. Mecerreyes and M. Antonietti, *Prog. Polym. Sci.*, 2013, **38**, 1009–1036.
18 W. J. Qian, J. Texter and F. Yan, *Chem. Soc. Rev.*, 2017, **46**, 1124–1159.
19 L. J. Li, T. A. Pascal, J. G. Connell, F. Y. Fan, S. M. Meckler, L. Ma, Y. M. Chiang, D. Prendergast and B. A. Helms, *Nat. Commun.*, 2017, **8**, 2277.
20 E. Josef, Y. Yan, M. C. Stan, J. Wellmann, A. Vizintin, M. Winter, P. Johansson, R. Dominko and R. Guterman, *Isr. J. Chem.*, 2019, **59**, 832–842.
21 G. R. Li, F. Lu, X. Y. Dou, X. Wang, D. Luo, H. Sun, A. P. Yu and Z. W. Chen, *J. Am. Chem. Soc.*, 2020, **142**, 3583–3592.
22 S. Q. Dai, C. Z. Wang, C. Y. Huang, S. R. Li, Y. S. Xu, Y. H. Song, G. J. Zeng, J. Zhu, T. L. Sun and M. J. Huang, *Macromol. Rapid Commun.*, 2023, **44**, e2200246.
23 Y. H. Lee, J. H. Kim, J. H. Kim, J. T. Yoo and S. Y. Lee, *Adv. Funct. Mater.*, 2018, **28**, 1801422.
24 X. Liu, Y. Lu, Q. H. Zeng, P. P. Chen, Z. F. Li, X. Wen, W. Wen, Z. X. Li and L. Y. Zhang, *ChemSusChem*, 2020, **13**, 715–723.
25 A. Vizintin, R. Guterman, J. Schmidt, M. Antonietti and R. Dominko, *Chem. Mater.*, 2018, **30**, 5444–5450.
26 L. J. Li, T. A. Pascal, J. G. Connell, F. Y. Fan, S. M. Meckler, L. Ma, Y. M. Chiang, D. Prendergast and B. A. Helms, *Nat. Commun.*, 2017, **8**, 2277.
27 Y. Gao, Z. J. Yan, J. L. Gray, X. He, D. W. Wang, T. H. Chen, Q. Q. Huang, Y. C. Li, H. Y. Wang, S. H. Kim, T. E. Mallouk and D. Wang, *Nat. Mater.*, 2019, **18**, 384–389.
28 L. S. Wu, J. P. Hu, S. J. Chen, X. R. Yang, L. Liu, J. S. Foord, P. Pobedinskas, K. Haenen, H. J. Hou and J. K. Yang, *Electrochim. Acta*, 2023, **466**, 142973.
29 Y. Shimoda, Y. Matsui, T. Tonoya and M. Ishikawa, *ACS Appl. Energy Mater.*, 2023, **6**, 8909–8918.
30 Q. Li, X. Zhao, S. Cao, L. Li, J. Li and F. Wu, *J. Alloys Compd.*, 2023, **960**, 170783.
31 A. Kim, S. H. Oh, A. Adhikari, B. R. Sathe, S. Kumar and R. Patel, *J. Mater. Chem. A*, 2023, **11**, 7833–7866.
32 W. B. Wang, Y. T. Zhang, H. C. Jiang, R. J. Zhang, N. Wang, Y. Y. Dou, Z. Y. Zhao, X. Yang, X. Y. Fan, X. D. Li, X. M. Guo, Q. L. Feng and S. L. Qiao, *Chem. Eng. J.*, 2023, **472**, 144888.
33 Z. Li, Y. Li, C. X. Bi, Q. K. Zhang, L. P. Hou, X. Y. Li, J. Ma, X. Q. Zhang, B. Q. Li, R. Wen and Q. Zhang, *Adv. Funct. Mater.*, 2023, **33**, 2304541.

© 2024 The Author(s). Published by the Royal Society of Chemistry

Open Access Article. Published on 07 March 2024. Downloaded on 2/7/2026 9:32:35 PM. This article is licensed under a Creative Commons Attribution-NonCommercial 3.0 Unported Licence.

34 X. B. Cheng, R. Zhang, C. Z. Zhao and Q. Zhang, *Chem. Rev.*, 2017, **117**, 10403–10473.
35 H. J. Yang, C. Guo, A. Naveed, J. Y. Lei, J. Yang, Y. N. Nuli and J. L. Wang, *Energy Storage Mater.*, 2018, **14**, 199–221.
36 R. G. Cao, W. Xu, D. P. Lv, J. Xiao and J. G. Zhang, *Adv. Energy Mater.*, 2015, **5**, 1402273.
37 F. R. Zhang, Y. Y. Sun, Z. C. Wang, D. S. Fu, J. Li, J. C. Hu, J. J. Xu and X. D. Wu, *ACS Appl. Mater. Interfaces*, 2020, **12**, 23774–23780.
38 L. Liang, W. F. Yuan, X. H. Chen and H. Y. Liao, *Chem. Eng. J.*, 2021, **421**, 130000.
39 J. Y. Wu, Z. X. Rao, X. T. Liu, Y. Shen, C. Fang, L. X. Yuan, Z. Li, W. X. Zhang, X. L. Xie and Y. H. Huang, *Adv. Mater.*, 2021, **33**, e2007428.
40 X. Y. Fan, S. Chen, W. B. Gong, X. D. Meng, Y. C. Jia, Y. L. Wang, S. Hong, L. Zheng, L. R. Zheng, C. W. Bielawski and J. Geng, *Energy Storage Mater.*, 2021, **41**, 14–23.
41 H. Wang, Z. Cui, S. A. He, J. Zhu, W. Luo, Q. Liu and R. Zou, *Nano-Micro Lett.*, 2022, **14**, 189.
42 Z. Y. Dong, C. R. Zhang, H. W. Peng, J. Gong, H. Wang, Q. Zhao and J. Y. Yuan, *Mater. Horiz.*, 2020, **7**, 2683–2689.
43 Z. Y. Dong, C. R. Zhang, H. W. Peng, J. Gong and Q. Zhao, *J. Mater. Chem. A*, 2020, **8**, 24493–24500.
44 J. Zhang, Z. Y. Chen, Y. Zhang, S. Y. Dong, Y. F. Chen and S. G. Zhang, *Adv. Mater.*, 2021, **33**, e2100962.
45 Z. H. Luo, W. J. Li, J. P. Yan and J. Sun, *Adv. Funct. Mater.*, 2022, **32**, 2203988.
46 Y. J. Yang, R. Wang, J. X. Xue, F. Q. Liu, J. Yan, S. X. Jia, T. Q. Xiang, H. Huo, J. J. Zhou and L. Li, *J. Mater. Chem. A*, 2021, **9**, 27390–27397.
47 R. Chu, T. T. Nguyen, Y. Bai, N. H. Kim and J. H. Lee, *Adv. Energy Mater.*, 2022, **12**, 2102805.
48 J. Yan, F. Q. Liu, J. Gao, W. Zhou, H. Huo, J. J. Zhou and L. Li, *Adv. Funct. Mater.*, 2021, **31**, 2007255.
49 Z. Y. Hu, F. Q. Liu, J. Gao, W. D. Zhou, H. Huo, J. J. Zhou and L. Li, *Adv. Funct. Mater.*, 2019, **30**, 1907020.
50 Q. Jin, K. X. Zhao, L. Wu, L. L. Li, L. Kong and X. T. Zhang, *J. Energy Chem.*, 2023, **84**, 22–29.
51 X. J. Weng, Y. Y. Qin, X. Y. Da, Y. J. Zhao, X. T. Deng, B. Wen, M. Y. Cui, X. K. Yin, Y. Q. Su, J. X. Song, S. J. Ding, X. F. Hu, G. X. Gao and X. F. Li, *Chem. Eng. J.*, 2023, **466**, 143302.
52 Q. D. Wang, Z. P. Yao, C. L. Zhao, T. Verhallen, D. P. Tabor, M. Liu, F. Ooms, F. Kang, A. Aspuru-Guzik, Y. S. Hu, M. Wagemaker and B. H. Li, *Nat. Commun.*, 2020, **11**, 4188.
53 L. K. Chen, T. Gu, J. B. Ma, K. Yang, P. R. Shi, J. Biao, J. S. Mi, M. Liu, W. Lv and Y. B. He, *Nano Energy*, 2022, **100**, 107470.
54 S. Kim, S. O. Park, M. Y. Lee, J. A. Lee, I. Kristanto, T. K. Lee, D. Hwang, J. Kim, T. U. Wi, H. W. Lee, S. K. Kwak and N. S. Choi, *Energy Storage Mater.*, 2022, **45**, 1–13.
55 M. S. Kim, Z. Zhang, J. Wang, S. T. Oyakhire, S. C. Kim, Z. Yu, Y. Chen, D. T. Boyle, Y. Ye, Z. Huang, W. Zhang, R. Xu, P. Sayavong, S. F. Bent, J. Qin, Z. Bao and Y. Cui, *ACS Nano*, 2023, **17**, 3168–3180.
56 X. Ji, S. Y. Hou, P. F. Wang, X. Z. He, N. Piao, J. Chen, X. L. Fan and C. S. Wang, *Adv. Mater.*, 2020, **32**, e2002741.
57 Y. Y. Feng, Y. Li, J. Lin, H. Y. Wu, L. Zhu, X. Zhang, L. L. Zhang, C. F. Sun, M. X. Wu and Y. B. Wang, *Nat. Commun.*, 2023, **14**, 3639.
58 Z. W. Seh, Y. Sun, Q. Zhang and Y. Cui, *Chem. Soc. Rev.*, 2016, **45**, 5605–5634.
59 Y. Gong, J. Li, K. Yang, S. Y. Li, M. Xu, G. P. Zhang, Y. Shi, Q. Cai, H. Li and Y. L. Zhao, *Nano-micro Lett.*, 2023, **15**, 150.
60 X. R. Chen, B. C. Zhao, C. Yan and Q. Zhang, *Adv. Mater.*, 2021, **33**, e2004128.
61 B. R. Li, Y. Chao, M. C. Li, Y. B. Xiao, R. Li, K. Yang, X. C. Cui, G. Xu, L. Li, C. K. Yang, Y. Yu, D. P. Wilkinson and J. J. Zhang, *Electrochem. Energy Rev.*, 2023, **6**, 7.
62 J. Y. Wei, X. Q. Zhang, L. P. Hou, P. Shi, B. Q. Li, Y. Xiao, C. Yan, H. Yuan and J. Q. Huang, *Adv. Mater.*, 2020, **32**, e2003012.
63 S. Nanda, A. Bhargav, Z. Jiang, X. H. Zhao, Y. Y. Liu and A. Manthiram, *Energy Environ. Sci.*, 2021, **14**, 5423–5432.
64 R. Wang, J. L. Yang, X. Chen, Y. Zhao, W. G. Zhao, G. Y. Qian, S. N. Li, Y. G. Xiao, H. Chen, Y. S. Ye, G. M. Zhou and F. Pan, *Adv. Energy Mater.*, 2020, **10**, 1903550.
65 M. I. Nandasiri, L. E. Camacho-Forero, A. M. Schwarz, V. Shutthanandan, S. Thevuthasan, P. B. Balbuena, K. T. Mueller and V. Murugesan, *Chem. Mater.*, 2017, **29**, 4728–4737.
66 Y. L. Lin, S. Huang, M. Xiao, D. M. Han, Z. H. Huang, S. J. Wang and Y. Z. Meng, *ACS Appl. Mater. Interfaces*, 2022, **14**, 22197–22205.
67 Y. Liu, H. W. Liu, Y. T. Lin, Y. X. Zhao, H. Yuan, Y. P. Su, J. F. Zhang, S. Y. Ren, H. Y. Fan and Y. G. Zhang, *Adv. Funct. Mater.*, 2021, **31**, 2104863.
68 F. Q. Liu, Z. Y. Hu, J. X. Xue, H. Huo, J. J. Zhou and L. Li, *RSC Adv.*, 2019, **9**, 40471–40477.
69 Z. Y. Zhao, X. B. Duan, L. Zhang, Z. W. Che, K. Wang, B. Zheng and X. G. Wang, *RSC Adv.*, 2021, **11**, 30755–30762.

© 2024 The Author(s). Published by the Royal Society of Chemistry